Progress In Electromagnetics Research C, Vol. 113, 97–110, 2021

Octa-Band Metamaterial Inspired Multiband Monopole Antenna for Wireless Application

Samuel Prasad Jones Christydass[1, 2, *] and Nagarajan Gunavathi[2]

Abstract—In this paper, a Rectangular Monopole Antenna (RMPA) with offset microstrip feed is presented. The structure is fabricated on an FR4 substrate with a dimension of $28 \times 32 \times 1.6\,\text{mm}^3$. The proposed structure achieves multiband operation by engraving 2 Complementary Split Ring Resonators (CSRRs) and a C-Shaped slot. Also, 2 Split Ring Resonators (SRRs) are printed on the adjacent sides of the radiating element. The parametric analysis is used to determine the optimum position of the feed and other critical parameters. The proposed structure operates at 2.25 GHz, 3.86 GHz, 4.60 GHz, 5.64 GHz, 5.86 GHz, 6.94 GHz, 7.48 GHz, and 9.47 GHz. The permeability of the SRR and permittivity of the CSRR are extracted and presented. The proposed antenna is fabricated and measured. The measured results of S_{11}, radiation pattern, and gain are on par with the simulated results. The proposed antenna's simulated surface current and efficiency are also presented to validate the performance. Simple structure, stable radiation pattern, multiband operation, reasonable gain, and efficiency are the significant features of the proposed RMPA.

1. INTRODUCTION

With the rapid development in multifunctional and integrated wireless communication systems, multiband antenna is widely required to cover different operating frequency bands. Some effective methods have been developed to achieve dual-bands [1], triple bands [2], quad-bands, and Penta bands [3–6]. Variety of techniques are available in the literature using such as slots [7], monopole arms [8], defected ground structure (DGS) [9, 10], etching slits [11], L-shaped notch [12], parasitic element [13], and rectangular slot [14].

Complex permittivity and permeability are used to represent all the materials in frequency domain. These parameters will determine the behavior of the material in the electromagnetic environment. The metamaterials exhibiting negative permittivity and permeability are also called left-handed (LH) materials. Many electromagnetism (EM) investigators modify LH material properties to achieve good EM properties required for many applications [15–17]. These metamaterials (MTM) have interesting EM properties which are certainly not available in nature. MTM inspires the structure with single or multiple unit cells and provides greater flexibility for getting various EM phenomena. Vaselago [18] first proposed the concept of MTM in 1967. These MTM structures have an unusual property of consecutive negative parameters called negative permeability and permittivity. MTM derives its properties from its structures with the size of the unit cell less than the guided wavelength ($P < \lambda_g/4$). Under such homogeneity conditions, these materials possess an excellent EM property that constructively disturbs the EM wave propagation and can be utilized for designing filters, couplers antennas, and devices used for communication [19–23]. Various classes of unit cells are based on split ring resonator [24], complementary split-ring resonator [26, 27], omega-shaped [25], and spiral resonator [28].

Received 11 April 2021, Accepted 5 June 2021, Scheduled 11 June 2021
* Corresponding author: Samuel Prasad Jones Christydass (prasadjoness.ece@krct.ac.in).
[1] Department of ECE, K. Ramakrishnan College of Technology, Trichy, Tamil Nadu 621112, India. [2] Department of ECE, National Institute of Technology, Trichy, Tamilnadu 621216, India.

In [29], a D-shaped CSRR is loaded in the ground plane to achieve dual-band operation at 2.48 GHz (2.41–2.56 GHz) and 3.16 GHz (3.12–3.18 GHz), which can be used for WLAN and Wi-MAX applications, respectively. In [30], an NB-CSRR loaded rectangular microstrip patch antenna is proposed for triple-band operation. A semicircular monopole antenna with two C-shaped slots and CSRR loaded ground plane is proposed for GSM, WiMAX, and C-band applications in [31]. Multiband antenna performance is achieved by using a triangular complementary split-ring resonator in [32], and the circularly polarized antenna is designed with CSRRs loaded on both patch and ground [33]. In [34], multiple circular CSRRs are introduced in the circular patch fed with meandered CPW feed to achieve tri-band application. A reconfigurable slot antenna is proposed in [35] for multiband operation, and in [36] a slot antenna for ISM band medical application is presented. In [37], an inverted patch with C-shaped construction, spiral slots, and a rectangular slot is used to achieve circular polarization, and in [38] a meandered slot with CPW is used to archive the wide bandwidth. However, all the work reported in the literature has a complex design, irregular radiation pattern, and minimum number of operating bands.

In this paper, we report a novel SRR and CSRR inspired octa-band RMPA. The step-by-step design procedures of the proposed RMPA are presented in Section 2. In Section 3, the parametric analysis is done to determine the various critical values of the proposed antenna. It is also validated that the multiband operation [39–43] is due to SRR and CSRR in Section 4. In Section 5, the simulated results are compared to the measured ones, followed by the article conclusion in Section 6.

2. PROPOSED RMPA CONFIGURATION

The proposed antenna is printed on an FR4 substrate with a dielectric constant of 4.4. The length and width of the substrate on which the radiating element is printed are 32 mm and 28 mm. The proposed antenna has 6 evolution steps, and it is shown in Figure 1. The parameters of the proposed antenna and its corresponding values are represented in Figure 2.

Antenna A is a simple rectangular monopole antenna with 20 mm and 14 mm as the length and width of the radiating element, which has the dual-band operation at 6.18 GHz (6.03–6.3327 GHz) and 8.83 GHz (8.7020–8.98 GHz). Antenna B is the RMPA with a CSRR etched on the right side of the radiating element, which resonates at three different frequencies 5.91 GHz (5.8216–6.008 GHz), 7.23 GHz (6.88–7.65 GHz), and 8.77 GHz (8.6413–8.88 GHz). With the introduction of CSRR, the resonant bands are shifted to the lower side because of the electric field coupling and resonant length increase. Antenna C is the RMPA with a CSRR etched on the left side of the radiating element, which has a dual-band operation at 2.72 GHz (2.7164–2.7796 GHz) and 5.99 GHz (5.8637–6.7072 GHz). A new resonance is created because of the introduction of CSRR in the radiating element, which exhibits negative permittivity at 2.72 GHz. Antenna D is the RMPA with a CSRR etched at both the left and right sides of the radiating element, which has a quad-band operation with resonating bands of 2.58 GHz (2.5396–2.6263 GHz), 5.46 GHz (5.40–5.5 GHz), 5.79 GHz (5.6864–5.9088 GHz), and 8.16 GHz (8.001–8.3467 GHz). Antenna E is the Antenna D with a C-shaped slot at the top of the radiating element, which also operates in the quad-bands at 2.5 GHz (2.47–2.55 GHz), 5.68 GHz (5.5571–5.567 GHz), 8.28 GHz (8.1092–8.4279 GHz), and 9.31 GHz (9.2184–9.4108 GHz). Antenna F is the modified version of Antenna E, in which two SRRs are printed along the sides of the radiating element, and they are connected to the radiating element. This antenna F has octa-band operation with resonances at 2.25 GHz (2.1951–2.2654 GHz), 3.86 GHz (3.83–3.914 GHz), 4.60 GHz (4.54–4.65 GHz), 5.64 GHz (5.89–5.73 GHz), 5.86 GHz (5.80–5.92 GHz), 6.94 GHz (6.83–7.057 GHz), 7.48 GHz (7.3173–7.6341 GHz) and 9.47 GHz (9.3293–9.6141 GHz).

The double-sided copper-clad FR4 substrate is cleaned with acetone. The structure is laminated with a photoresist film after being dried up. Then the mask, which is the negative of the proposed design, is attached to the photoresist laminated FR4 substrate and exposed to UV light. Then the substrate is dissolved in sodium carbonate developer solution and etching process using ferric chloride solution. Then the sodium hydroxide is used to remove the hardened photoresist to develop the proposed antenna shown in Figure 11. The comparison of the various multiband antenna with the proposed antenna is tabulated in Table 1. It could be inferred from Table 1 that the proposed antenna is an excellent candidate for the multifunctional communication device since it operates in eight bands.

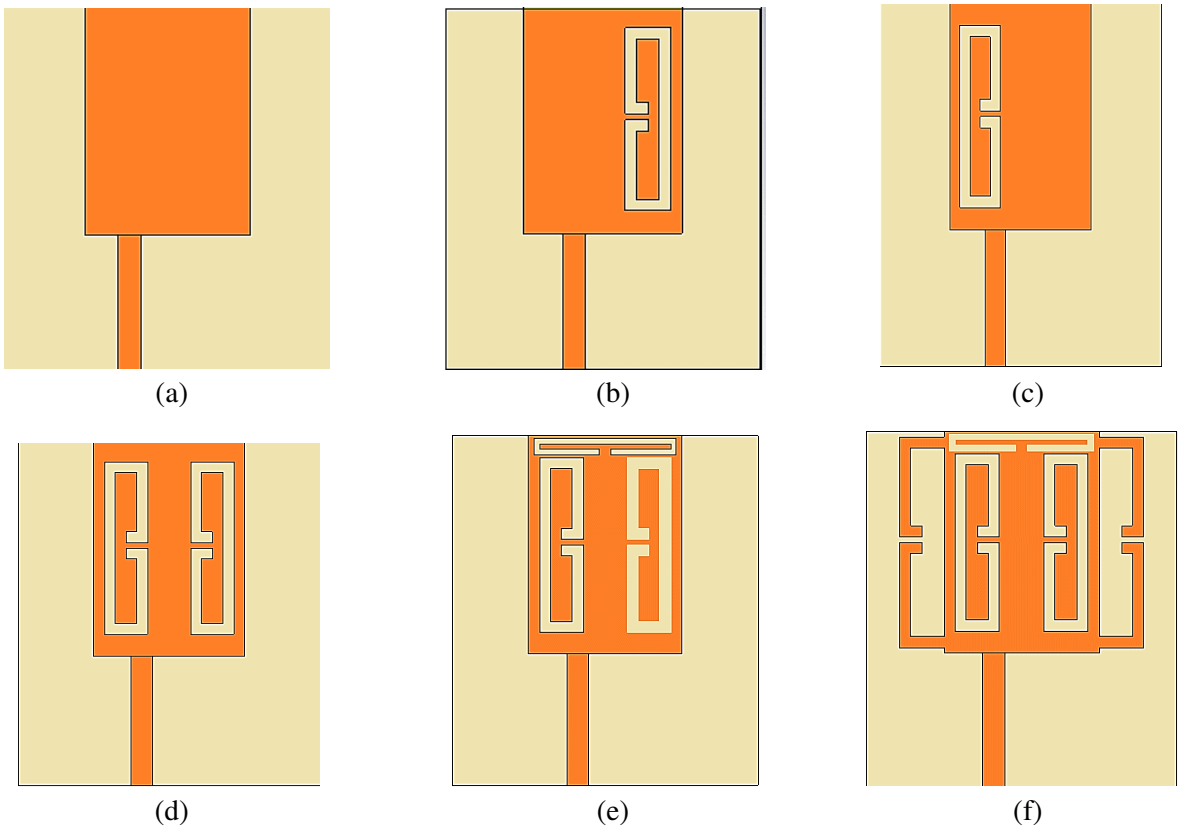

Figure 1. Evolution of proposed RMPA. (a) Antenna A, (b) Antenna B, (c) Antenna C, (d) Antenna D, (e) Antenna E, (f) Antenna F.

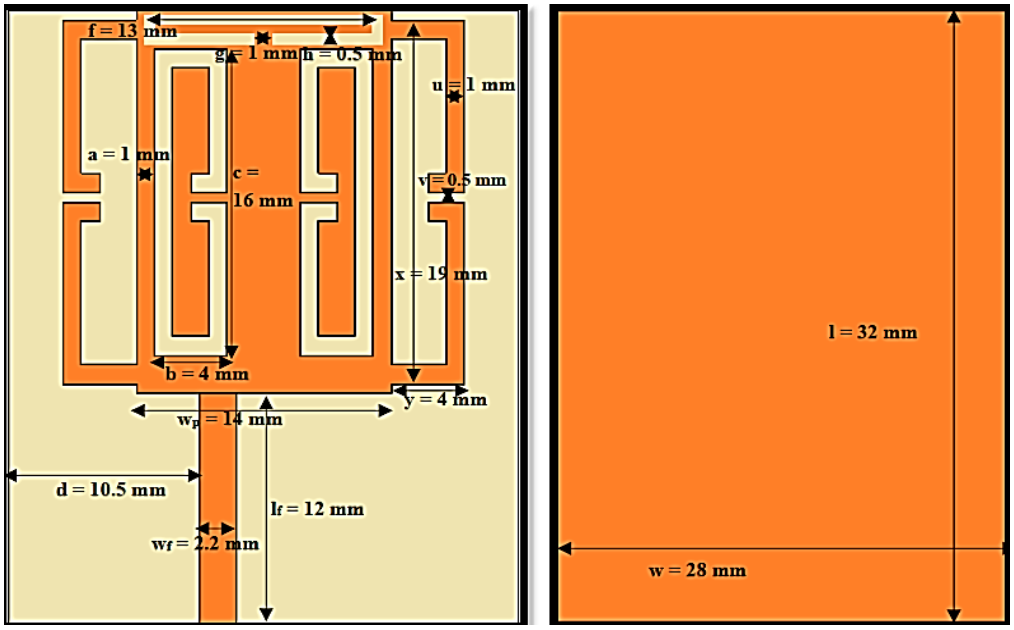

Figure 2. Geometry of the proposed RMPA.

Table 1. Multiband antenna in literature vs our work.

Ref No	Technique	No. of Bands	Dimension	Resonating Frequency	Impedance Bandwidth
			mm^2	GHz	MHz
7	Hexagonal slot	2	25×25	5.25	2120
				6.73	6100
8	Monopole Arm	3	22×35	1.57	220
				2.02	200
				2.55	90
9	Slit	3	40×25	2.17	70
				3.38	70
				5.53	230
10	DGS	4	58×62	2.4	70
				3.5	76
				6	60
				6.7	50
11	Slit in ground	5	70×53	1.55	150
				2.92	1090
				4.32	220
				5.3	160
				5.78	190
our work	SRR and CSRR	8	28×32	2.25	70.3
				3.86	84
				4.6	110
				5.64	140
				5.86	120
				6.94	227
				7.48	316.8
				9.47	284.8

3. PARAMETRIC ANALYSIS

The parametric analysis of the proposed RMPA is done to select the optimized value. The feed position, feed width, and ground length are included for the parametric analysis, and the result and its inferences are discussed in this section.

The position of the feed is altered to select the optimum position. Figure 3 clearly shows that the feed position in the left end yields suitable impedance matching in all bands compared with the centers feed position and the feed in the right end.

Next, the width of the feed is increased in steps of 0.2 mm from 1.8 mm to 2.2 mm. It is revealed from Figure 4 that, with the increase in width of the feed, a perfect impedance matching is achieved for all the operating bands except at the higher band, hence the optimum value of 2.2 mm is chosen for the width of the feed. When the length of the ground is varied as half ground, 3/4 of the ground, and full ground, the proposed RMPA with full ground structure yields perfect impedance matching, and new bands are created. This is clearly depicted in Figure 5, and therefore, the full ground size is utilized for the final design.

After the optimum feed position is determined, the critical parameters of the metamaterial are

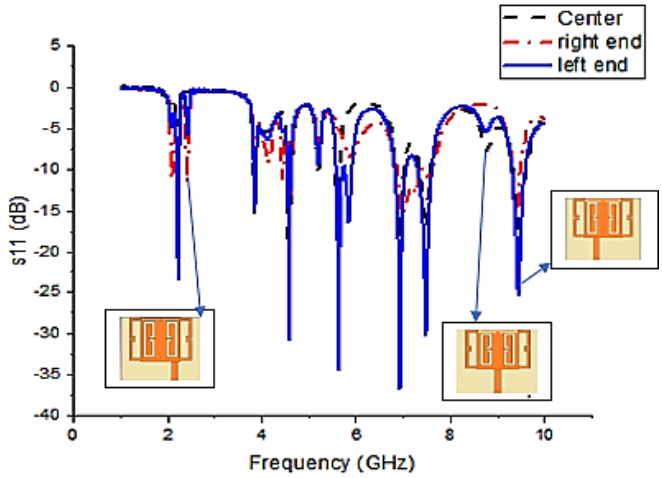

Figure 3. Simulated S_{11} for various feed positions of the proposed RMPA.

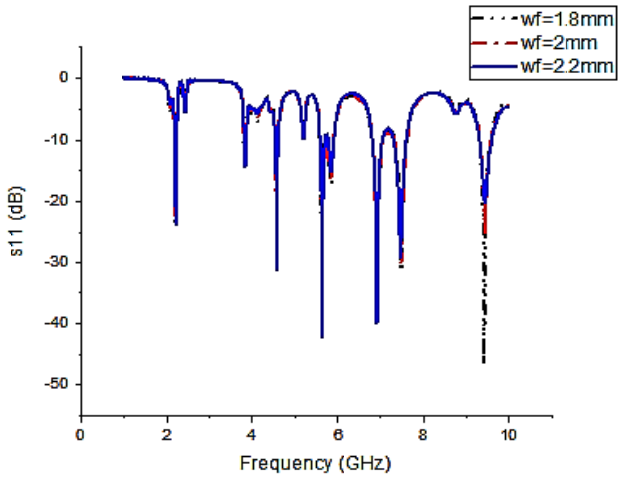

Figure 4. Simulated S_{11} for various feed width of the proposed RMPA.

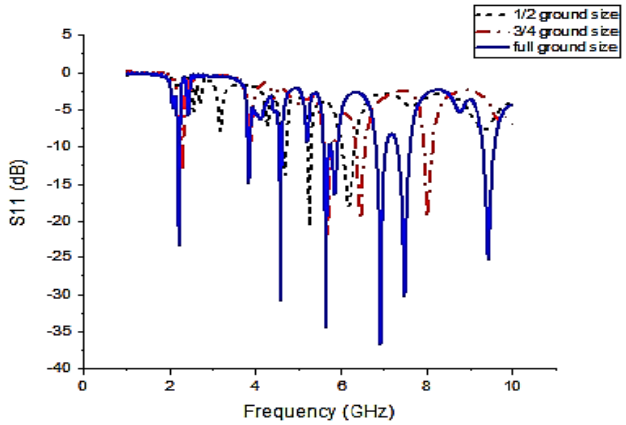

Figure 5. Simulated S_{11} for various length of the ground.

chosen based on the parametric analysis. The parameter chosen for the analysis is a, g, and v. The value of a is increased in steps of 0.5 mm from 0.5 mm to 1.5 mm. The analysis is presented in Figure 6, and we observe that $a = 1$ mm has good impedance matching in all the resonating bands. The 3.86 GHz and 5.65 GHz bands are highly affected when the value of a is varied, and hence the CSRR etched is the reason for these operating bands. It is also validated with the surface current distribution presented in Section 5, where the maximum current is around the CSRR at the respective bands. In Figure 7, the return loss for various g is presented, and we can observe that $g = 1$ mm maintains good matching and impedance bandwidth in all the resonating bands. The band at 9.47 GHz is shifted as the value of the g is varied, and the surface current is highly concentrated around the C-slot at this frequency.

In Figure 8, the simulated return loss plot for various values v is presented; from that, we observe that $v = 0.5$ mm has good matching in all the resonating bands. The two bands, 2.25 GHz and 7.48 GHz, are affected due to the inclusion of adjacent SRR. So, for the final fabrication, $a = 1$ mm, $g = 1$ mm, and $v = 0.5$ mm are chosen. In Figure 9, the efficiency of the proposed antenna and its evolution stages is presented. The efficiency of the proposed antenna is above 65% of all the resonating bands and 90% as its maximum efficiency.

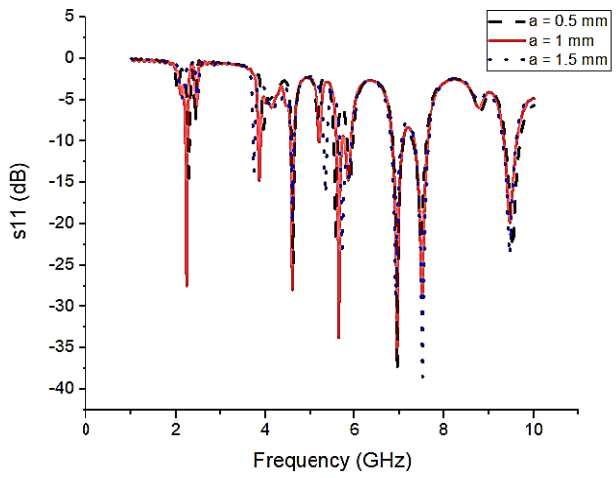

Figure 6. Simulated S_{11} for various values of a.

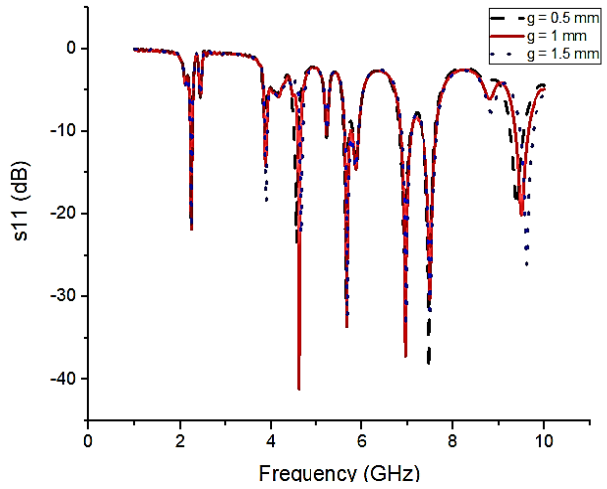

Figure 7. Simulated S_{11} for various values of g.

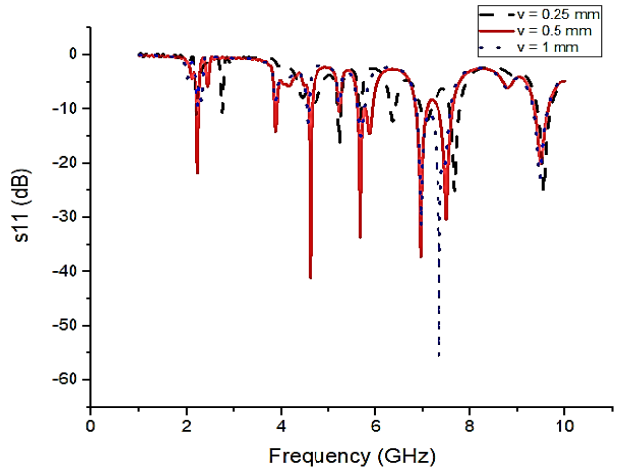

Figure 8. Simulated S_{11} for various values of v.

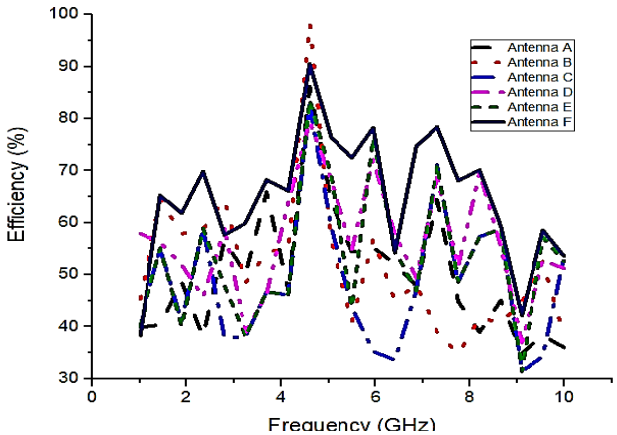

Figure 9. Efficiency of the proposed antenna.

4. EXTRACTION OF CONSECUTIVE PARAMETER

An appropriate boundary condition is defined for the extraction of the transmission and reflection coefficient. Through the input port, the EM wave is used to excite the SRR and CSRR. At the output port, the transmission and reflection coefficient is retrieved. The negative permeability of SRR and permittivity of CSRR are extracted with the help of the Nicolson-Ross-Weir (NRW) [44, 45] method

$$\mu_r = \frac{2}{jK_O d} * \frac{1 - V_2}{1 + V_2} \tag{1}$$

$$\varepsilon_r = \frac{2}{jK_O d} * \frac{1 - V_1}{1 + V_1} \tag{2}$$

where d is the thickness of the substrate, K_O the free space wavenumber, $V_1 = S_{21} - S_{11}$, and $V_2 = S_{21} + S_{11}$. The waveguide extraction setup, shown in Figure 10, is used to compute the reflection and transmission coefficient of the proposed antenna, which is presented in Figure 11. With the help of MATLAB coding, the negative permittivity and permeability of the proposed antenna are extracted.

At low frequency, the SRR will have capacitive nature; because of that, the induced magnetic field and the applied field will be in phase. Thus, SRR can have a permeability value greater than

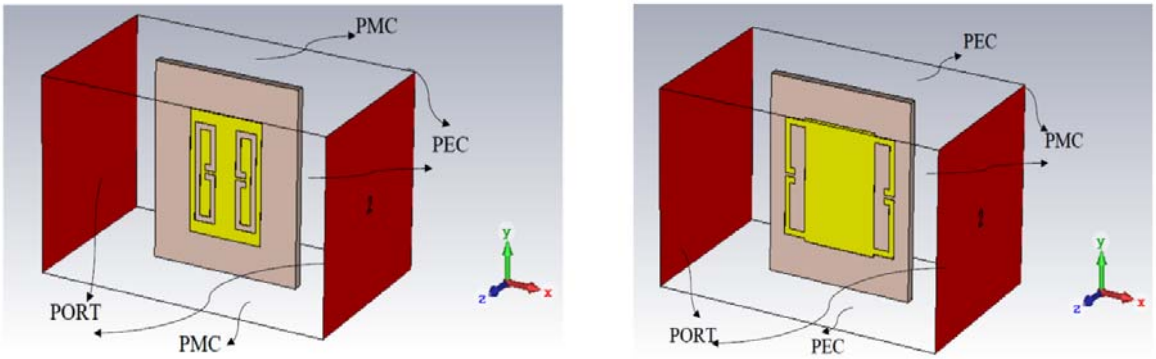

(a) (b)

Figure 10. Waveguide extraction method for retrieving S_{11} and S_{21}. (a) CSRR permittivity, (b) SRR permeability.

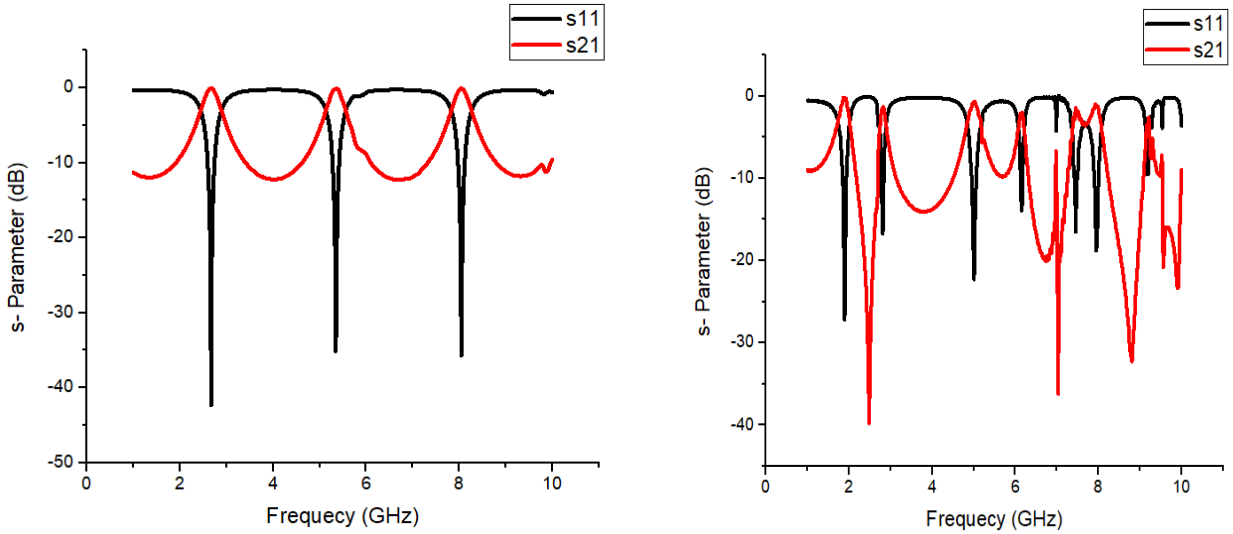

(a) (b)

Figure 11. S parameter (mag of S_{11} and S_{21}). (a) CSRR transmission & reflection coefficient, (b) SRR transmission & reflection coefficient.

1, and it resembles the magnetic dipole. While the CSRR acts as an inductor, CSRR can have a permittivity value greater than 1. Figure 12 depicts the permittivity of the CSRR and permeability of the SRR derived from the transmission and reflection coefficient of CSRR and SRR, respectively. We observe negative permittivity and permeability at various resonating frequencies. These properties are responsible for the multiband characteristics of the proposed antenna, which is clearly exposed in the S_{11} characteristics.

5. RESULT AND DISCUSSION

In Figure 13, the simulated surface current distributions at various operating frequencies are presented. It is clearly inferred from the surface current distributions that the current path is altered by the inclusion of CSRR, SRR, and C-shaped slot.

From Figure 13, it is clearly seen that the resonance at 3.86 GHz and 5.64 GHz is due to the etching of CSRR in the radiating element. Similarly, the 9.47 GHz resonance is due to the C-shaped slot at the

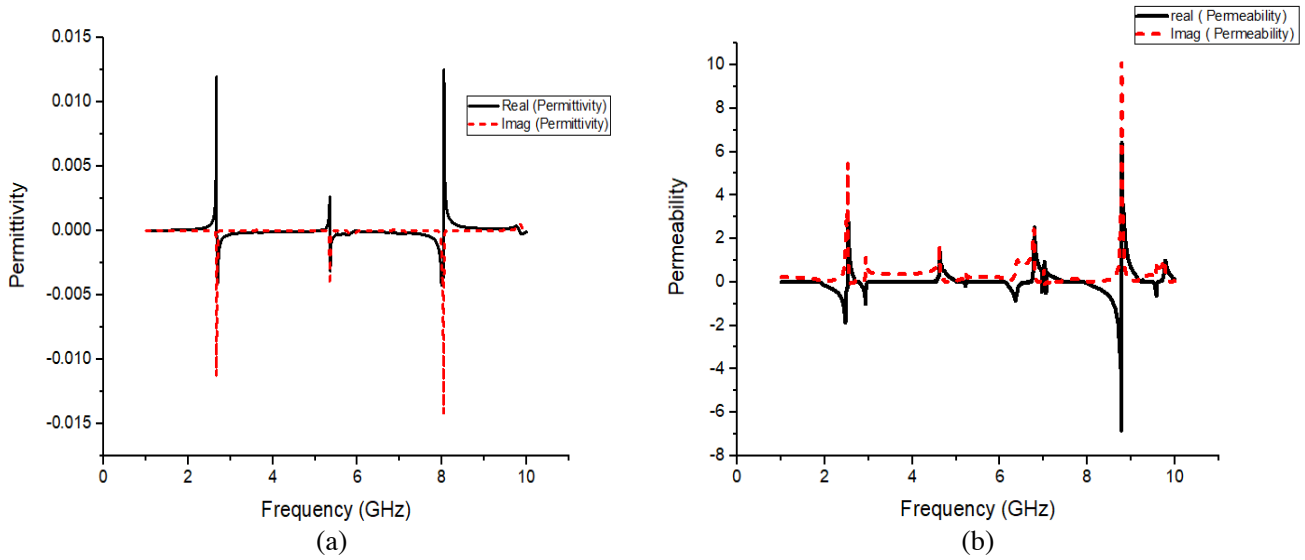

Figure 12. Metamaterial characteristics. (a) CSRR permittivity characteristics, (b) SRR permeability characteristics.

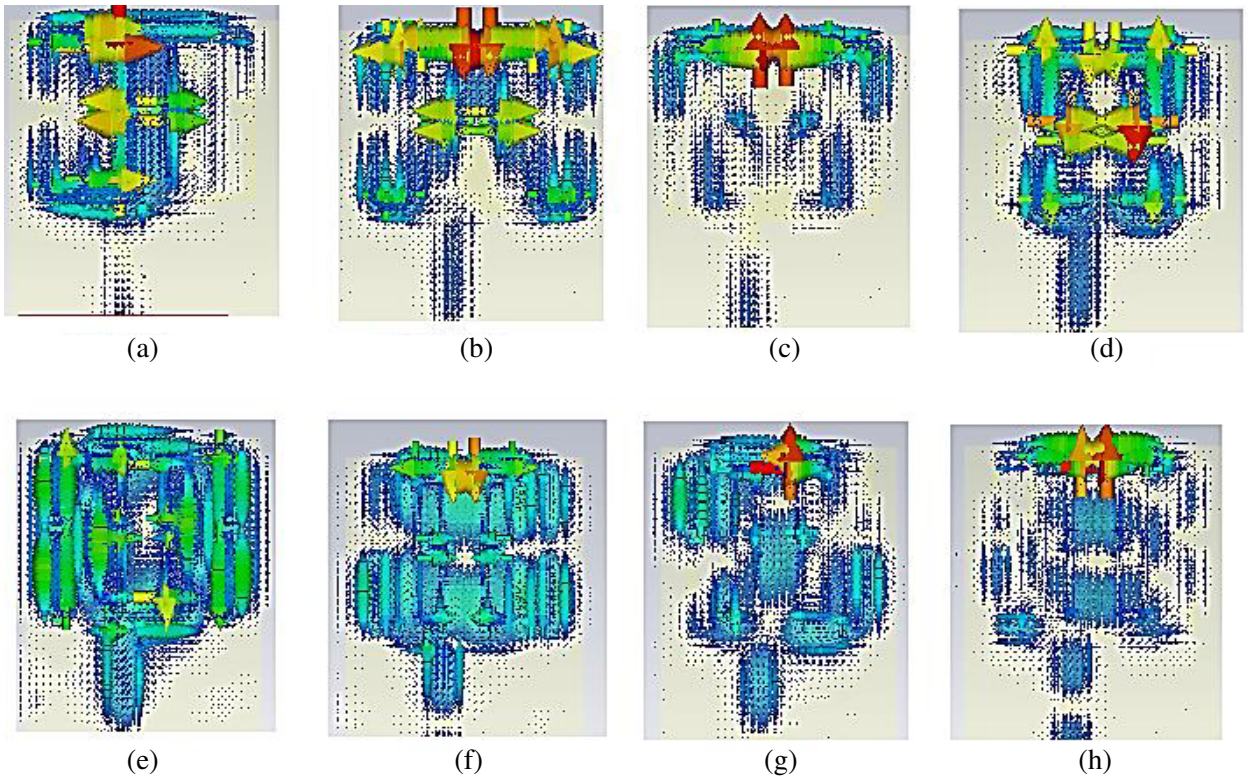

Figure 13. Simulated surface current at various resonating frequencies. (a) 2.2 GHz, (b) 3.86 GHz, (c) 4.6 GHz, (d) 5.64 GHz, (e) 5.86 GHz, (f) 6.94 GHz, (g) 7.48 GHz, (h) 9.47 GHz.

top of the radiating element. The resonance at 2.25 and 7.48 GHz is due to the inclusion of SRR at the adjacent side. The figure shows that the maximum current is around the metamaterial and slot at the respective resonant frequencies.

Horn antenna is considered as a transmitter source antenna, whereas the fabricated prototype is used as a receiver before being connected to a VNA Anritsu S820E via coaxial cable to measure the radiation patterns through a far-field measurement system which is located in an anechoic chamber. The two antennas are placed 1.25 m apart. In Figure 14, E-plane and H-plane simulated results are compared with measured results, and it is noted that the lower resonance has a similar pattern to a higher resonance. An omnidirectional H plane pattern and eight-shaped dipole E plane pattern are achieved in all the resonating bands by the proposed antenna. From the figure, it is viewed that

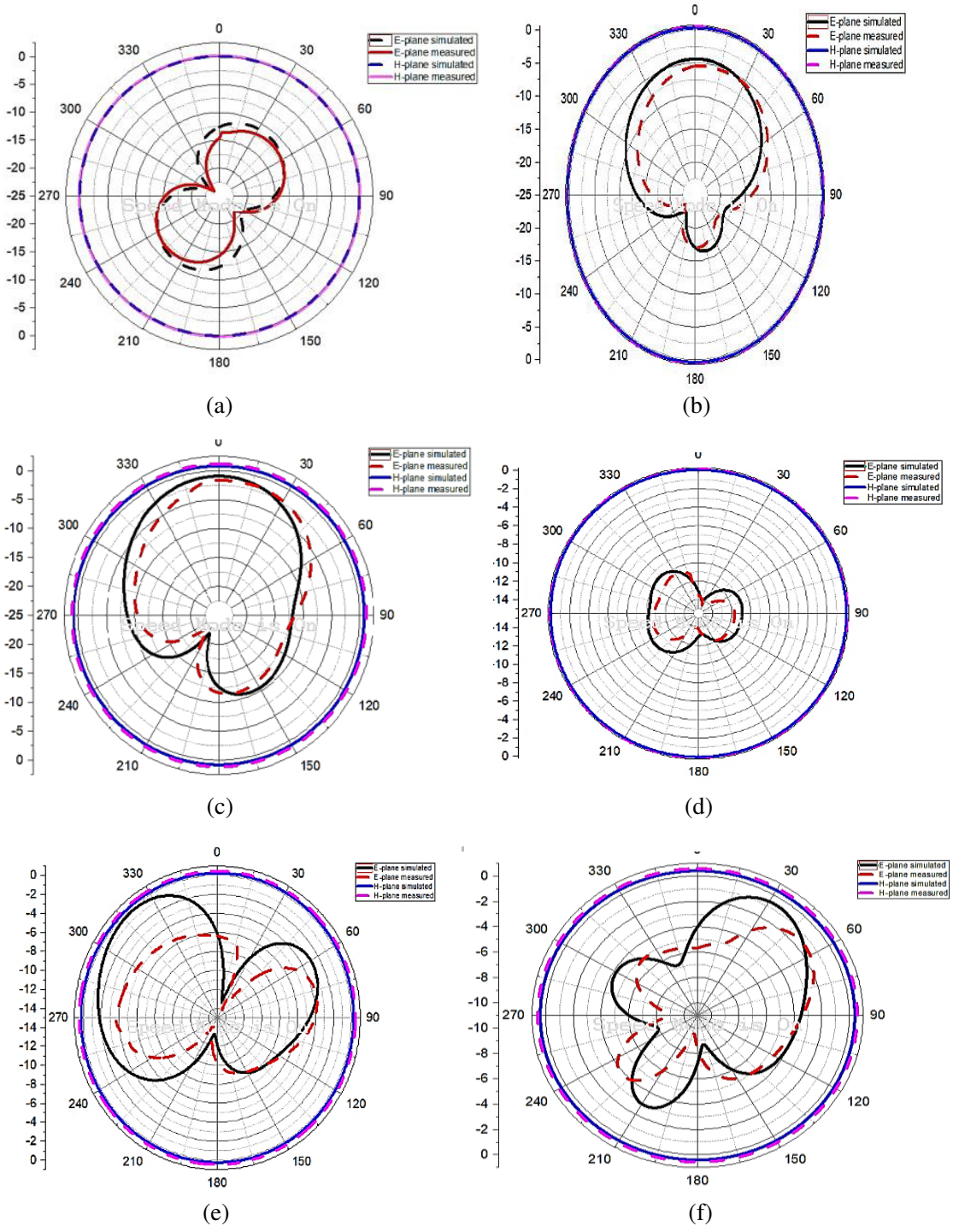

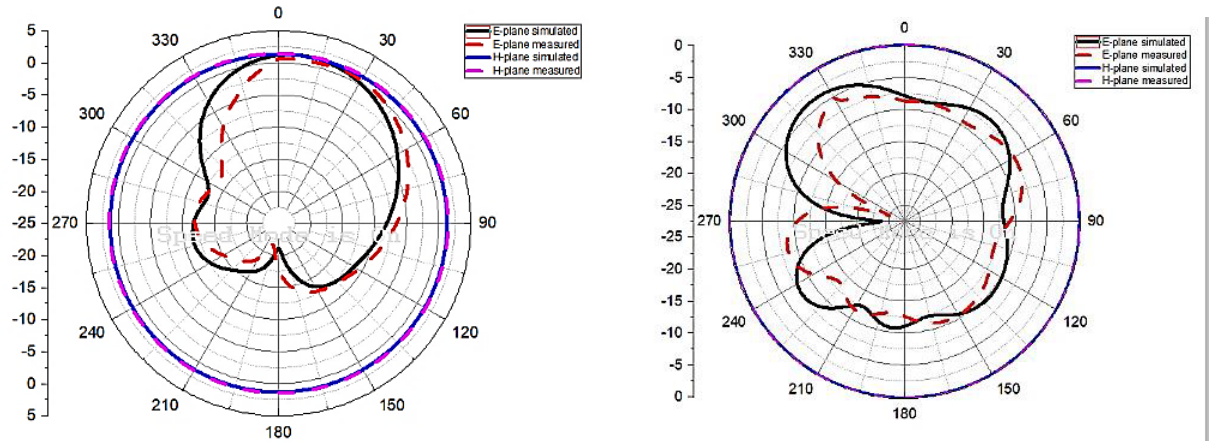

Figure 14. Simulated & measured radiation pattern. (a) 2.25 GHz, (b) 3.86 GHz, (c) 4.6 GHz, (d) 5.64 GHz, (e) 5.86 GHz, (f) 6.94 GHz, (g) 7.48 GHz, (h) 9.47 GHz.

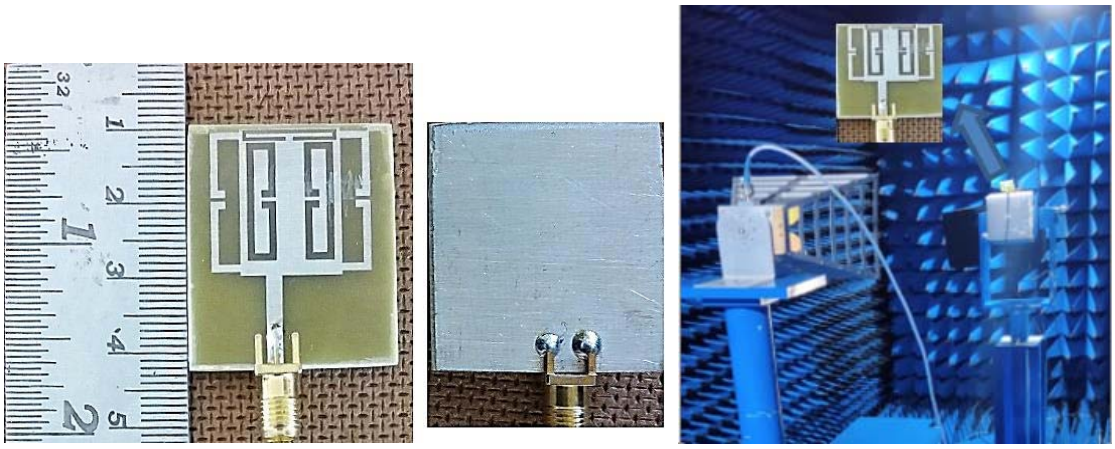

Figure 15. Top and bottom view of the fabricated antenna & measurement setup.

the radiation pattern is stable. The fabricated antenna is tested using the VNA Anritsu S820E. The measurement setup, top and rear views of the fabricated antenna are shown in Figure 15.

The return loss comparison for all the evolution stages of the proposed antenna is presented in Figure 16. We observe that the inclusion of the CSRR, SRR, and slot changes the current path, which in turn changes the resonant behavior of the proposed antenna at each stage. The final proposed structure antenna F is capable of operating at eight different frequencies of operations. It is evident from the figure that the inclusion of metamaterial structure (Split Ring Resonator and it is dual) and the slot is responsible for the multiband operation. The fabricated antenna is measured, and the results are compared with the simulated results. The compared result is presented in Figure 17, which is in the near pact. The observed deviation between the results is due to an error during fabrication and SMA soldiering. The measured gain is plotted with the simulated gain with respect to the frequency of operation in Figure 18. The proposed antenna achieves a good gain over the entire operating frequency. The proposed structure maintains gain above 1.5 dBi in all the resonating bands. The simulated and measured numerical data of the proposed antenna are tabulated in Table 2.

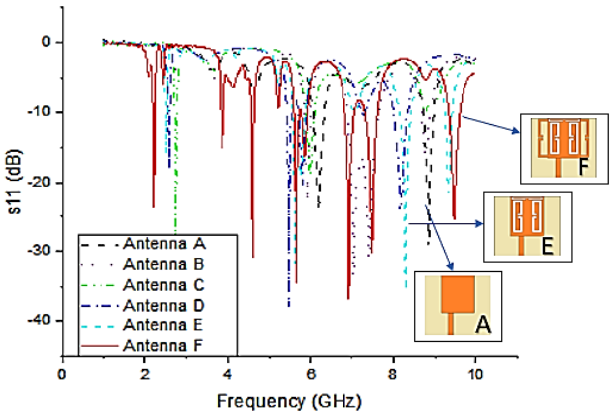

Figure 16. Comparison of simulated S_{11} characteristics.

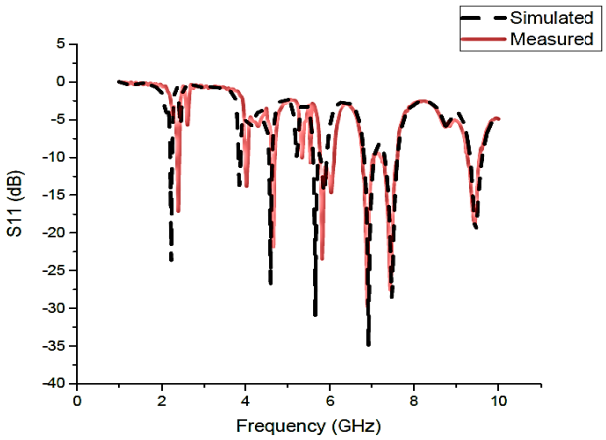

Figure 17. Simulated S_{11} vs measured S_{11}.

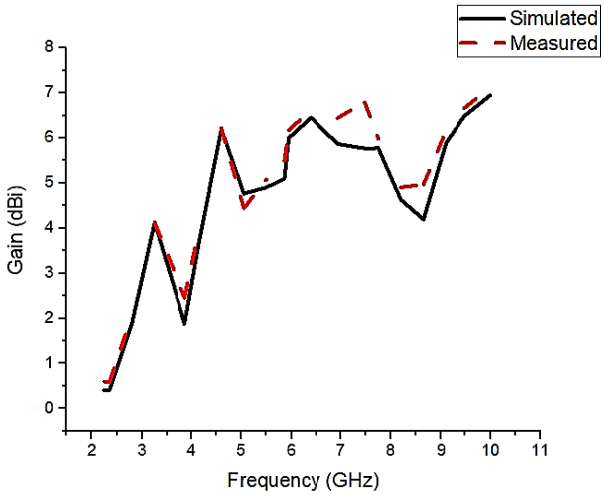

Figure 18. Simulated vs measured gain plotted against frequency.

Table 2. Simulated vs measured results.

Simulated					Measured				
Resonant Frequency	**Gain**	**Return loss**	**Operating band**	**Impedance Bandwidth**	**Resonant Frequency**	**Gain**	**Return loss**	**Operating band**	**Impedance Bandwidth**
(GHz)	(dBi)	(dB)	(GHz)	(MHz)	(GHz)	(dBi)	(dB)	(GHz)	(MHz)
2.25	0.403	−28.01	2.21–2.27	60	2.38	0.42	−17.48	2.35–2.41	60
3.86	1.87	−14.77	3.84–3.88	40	4.02	2.56	−13.92	3.98–4.06	80
4.6	6.19	−27.93	4.56–4.62	60	4.66	6.01	−22.93	4.60–4.68	72
5.64	4.98	−33.74	5.61–5.73	117	5.806	5.48	−24.89	5.76–6.09	333
5.86	5.16	−14.71	5.78–5.91	135	6.022	5.98	−14.71		
6.94	5.86	−35.93	6.83–7.06	234	6.904	6.51	−30.43	6.79–7.04	252
7.48	5.78	−28.86	7.31–7.60	288	7.444	6.41	−28.46	7.22–7.61	387
9.47	6.48	−19.82	9.33–9.61	279	9.451	6.53	−18.74	9.38–9.55	270

6. CONCLUSION

In this paper, a compact octa-band rectangular microstrip patch antenna is proposed with 6 evolutions. With the inclusion of CSRR, SRR, and C-shaped slots, multiband operations are achieved, which is the prerequisite for all multifunctional communication systems. The proposed antenna has a compact size of $28 \times 32 \times 1.6\,\text{mm}^3$ with 8 resonances at 2.25 GHz, 3.86 GHz, 4.6 GHz, 5.64 GHz, 5.86 GHz, 6.94 GHz, 7.48 GHz, and 9.47 GHz, and has a reasonable gain in all its operating bands. The efficiency is above 65% in all the resonating bands. The negative permittivity and permeability characteristics are extracted and presented. The simulated results are on par with the measured ones. The proposed RMPA has a low profile, simple structure, easy fabrication and integration into modern multifunctional wires systems.

REFERENCES

1. Jhamb, K., L. Li, and K. Rambabu, "Novel-integrated patch antennas with multiband characteristics," *IET Microwaves Antennas Propag.*, Vol. 5, 1393–1398, 2011.
2. Moosazadeh, M. and S. Kharkovsky, "Compact and small planar monopole antenna with symmetrical L- and U-shaped slots for WLAN/WiMAX applications," *IEEE Antennas Wireless Propag. Lett.*, Vol. 13, 388–391, 2014.
3. Mopidevi, H., Y. Damgaci, D. Rodrigo, L. Jofre, and B. A. Cetiner, "A quad-band antenna for public safety applications," *IEEE Antennas Wireless Propag. Lett.*, Vol. 13, 1231–1234, 2014.
4. Alsath, M. G. N. and M. Kanagasabai, "Planar pentaband antenna for vehicular communication application," *IEEE Antennas Wireless Propag. Lett.*, Vol. 13, 110–113, 2014.
5. Li, Y., Z. Zhang, Z. Feng, and M. F. Iskander, "Design of penta-band omnidirectional slot antenna with slender columnar structure," *IEEE Trans. Antennas Propag.*, Vol. 62, 594–601, 2014.
6. Abutarboush, H. F., R. Nilavalan, S. W. Cheung, and K. M. Nasr, "Compact printed multiband antenna with independent setting suitable for fixed and reconfigurable wireless communication systems," *IEEE Antennas Wireless Propag. Lett.*, Vol. 60, 3867–3874, 2012.
7. Boopathi Rani, R. and S. K. Pandey, "A parasitic hexagonal patch antenna surrounded by same shaped slot for WLAN, UWB applications with notch at vanet frequency band," *Microwave and Optical Technology Letters*, Vol. 58, 2996–3000, 2016.
8. Brar, R. S., K. Saurav, D. Sarkar, and K. V. Srivastava, "A triple band circular polarized monopole antenna for GNSS/UMTS/LTE," *Microwave and Optical Technology Letters*, Vol. 59, 298–303, 2017.
9. Rakesh Kumar, P., K. Satya Prasad, and A. Guruva Reddy, "Dual polygonal slit square patch with defected ground plane for tri band operation," *Microwave and Optical Technology Letters*, Vol. 59, 1071–1074, 2017.
10. Hosseini Varkiani, S. M. and M. Afsahi, "Grounded CPW multiband wearable antenna for MBAN and WLAN applications," *Microwave and Optical Technology Letters*, Vol. 60, 561–568, 2018.
11. Tuan Le, T., H. H. Tran, and H. C. Park, "A simple penta-band circularly polarized CPW-fed monopole-patch antenna covering six commercial application bands," *Microwave and Optical Technology Letters*, Vol. 60, 773–778, 2018.
12. Singh, V., B. Mishra, A. K. Dwivedi, and R. Singh, "Inverted L-notch loaded hexa band circular patch antenna for X, Ku/K band applications," *Microwave and Optical Technology Letters*, Vol. 60, 2081–2088, 2018.
13. Varma, R. and J. Ghosh, "Multiband proximity coupled microstrip antenna for wireless applications," *Microwave and Optical Technology Letters*, Vol. 60, 424–428, 2018.
14. Singh, V., B. Mishra, P. N. Tripathi, and R. Singh, "A compact quad-band microstrip antenna for S and C-band applications," *Microwave and Optical Technology Letters*, Vol. 58, 1365–1369, 2016.
15. Engheta, N. and R. W. Ziolkowski, *Metamaterials: Physics and Engineering Explorations*, IEEE Press, Wiley Publishing, Hoboken, NJ, 2006.
16. Eleftheriades, G. V. and K. G. Balmain, *Negative-refraction Metamaterials Fundamental Principles and Applications*, IEEE Press, Wiley Publishing, 2005.

17. Caloz, C. and T. Itoh, *Electromagnetic Metamaterials: Transmission Line Theory and Microwave Applications*, IEEE Press, Wiley Publishing, 2005.
18. Veselago, V. G., "Electrodynamics of substances with simultaneously negative electrical and magnetic properties," *Sov., Phys.*, Vol. 10, 509–517, February 1968.
19. Mehdipour, A., T. A. Denidni, and A.-R. Sebak, "Multiband miniaturized antenna loadedby ZOR and CSRR metamaterial structures with monopolar radiation pattern," *IEEE Trans. Antennas Propag.*, Vol. 62, 555–562, 2014.
20. Yoo, M. and S. Lim, "SRR and CSRR loaded ultra-wideband (UWB) antenna with tri-band notch capability," *Journal of Electromagnetic Waves and Applications*, Vol. 27, 2190–2197, 2013.
21. Xu, H.-X., G.-M. Wang, C.-X. Zhang, and Q. Peng, "Hilbert-shaped complementary single split ring resonator and low-pass filter with ultra-wide stopband, excellent selectivity and low insertion loss," *AEU-International Journal of Electronics and Communications*, Vol. 65, 901–905, 2011.
22. Hamidreza, M.-T., A. Ramesh, and N. Mohsen, "A cavity-backed antenna loaded with complimentary split ring resonators," *AEU-International Journal of Electronics and Communications*, Vol. 70, 928–935, 2016.
23. Phani Kumar, K. V. and S. S. Karthikeyan, "Wideband three section branch line coupler using triple open complementary split ring resonator and open stubs," *AEU-International Journal of Electronics and Communications*, Vol. 69, 1412–1416, 2016.
24. Elavarasi, C. and T. Shanmuganantham, "SRR loaded CPW-fed multiple band rose flower-shaped fractal antenna," *Microwave and Optical Technology Letters*, Vol. 58, 1720–1724, 2016.
25. Javid Asad, M., M. Farhan Shafique, and S. A. Khan, "Performance restoration of dielectric embedded antennas using omega like complementary split ring resonators," *Microwave and Optical Technology Letters*, Vol. 58, 357–362, 2017.
26. Falcone, F., J. Illescas, E. Jarauta, A. Estevez, and J. A. Marcotegui, "Analysis of stripline configurations loaded with complementary split ring resonators," *Microwave and Optical Technology Letters*, Vol. 55, 1250–1254, 2013.
27. Boopathi Rani, R. and S. K. Pandey, "Metamaterial-inspired printed UWB antenna for short range RADAR applications," *Microwave and Optical Technology Letters*, Vol. 59, 1600–1604, 2017.
28. Srivastava, K., A. Kumar, and B. K. Kanaujia, "Compact penta-band microstrip antenna," *Microwave and Optical Technology Letters*, Vol. 57, 836–883, 2016.
29. Singh, G., B. K. Kanaujia, V. K. Pandey, D. Gangwar, and S. Kumar, "Design of compact dual-band patch antenna loaded with D-shaped complementary split ring resonator," *Journal of Electromagnetic Waves and Applications*, Vol. 33, 2096–2111, 2019.
30. Pandeeswari, R., "A compact non-bianisotropic complementary split ring resonator inspired microstrip triple band antenna," *Progress In Electromagnetics Research C*, Vol. 81, 115–124, 2018.
31. Daniel, R. S., R. Pandeeswari, and S. Raghavan, "Multiband monopole antenna loaded with complementary split ring resonator and C-shaped slots," *AEU-International Journal of Electronics and Communications*, Vol. 75, 8–14, 2017.
32. Rajkumar, R. and U. K. Kommuri, "A triangular complementary split ring resonator based compact metamaterial antenna for multiband operation," *Wireless Personal Communications*, Vol. 101, 1075–1089, 2018.
33. Dey, S., S. Mondal, and P. P. Sarkar, "Single feed circularly polarized antenna loaded with complementary split ring resonator (CSRR)," *Progress In Electromagnetics Research M*, Vol. 78, 175–184, 2019.
34. Pandeeswari, R., "Complimentary split ring resonator inspired meandered CPW-fed monopole antenna for multiband operation," *Progress In Electromagnetics Research C*, Vol. 80, 13–20, 2018.
35. Ali, T., M. M. Khaleeq, and R. C. Biradar, "A multiband reconfigurable slot antenna for wireless applications," *AEU-International Journal of Electronics and Communications*, Vol. 84, 273–280, 2018.
36. Li, Y. J., Z. Y. Lu, and L. S. Yang, "CPW-fed slot antenna for medical wearable applications," *IEEE Access*, Vol. 7, 42107–42112, 2019.

37. Kumar, A., M. M. Sharma, and R. P. Yadav, "Dual wideband circular polarized CPW-fed strip and slots loaded compact square slot antenna for wireless and satellite applications," *AEU-International Journal of Electronics and Communications*, Vol. 108, 181–188, 2019.
38. Fang, X., G. Wen, D. Inserra, Y. Huang, and J. Li, "Compact wideband CPW-fed meandered-slot antenna with slotted Y-shaped central element for Wi-Fi, WiMAX, and 5G applications," *IEEE Trans. Antennas Propag.*, Vol. 66, 7395–7399, 2018.
39. Daniel, R. S., "Broadband μ-negative antenna using ELC unit cell," *AEU-International Journal of Electronics and Communications*, Vol. 1, 2020.
40. Selvi, N. T., P. T. Selvan, S. P. Babu, and R. Pandeeswari, "Multiband metamaterial-inspired antenna using split ring resonator," *Computers & Electrical Engineering*, Vol. 1, 2020.
41. Rajak, N., N. Chattoraj, and R. Mark, "Metamaterial cell inspired high gain multiband antenna for wireless applications," *AEU-International Journal of Electronics and Communications*, Vol. 1, 23–30, 2019.
42. Saraswat, R. K. and M. Kumar, "A metamaterial hepta-band antenna for wireless applications with specific absorption rate reduction," *International Journal of RF and Microwave Computer-Aided Engineering*, Vol. 29, 2019.
43. Anand, S. and P. Prashalee, "High gain compact multiband cavity-backed SIW and metamaterial unit cells with CPW feed antenna for S, and Ku band applications," *Wireless Personal Communications*, Vol. 26, 1–4, 2021.
44. Daniel, R. S. and R. Selvaraj, "A low-profile spilt ring monopole antenna loaded with hexagonal split ring resonator for RFID applications," *Progress In Electromagnetics Research M*, Vol. 92, 169–179, 2020.
45. Rothwell, E. J., J. L. Frasch, S. M. Ellison, P. Chahal, and R. O. Ouedraogo, "Analysis of the Nicolson-Ross-Weir method for characterizing the electromagnetic properties of engineered materials," *Progress In Electromagnetics Research*, Vol. 157, 31–47, 2016.